Electronic Supplementary Material (ESI) for Environmental Science: Nano.

Supplementary Information

Sea urchin-like plasma Ag/CAU-17@MoS_2 core-shell S-scheme heterojunctions with broad spectrum response and enhanced photothermal-photocatalysis

Xinyue Liu[a], Zipeng Xing[a*], Na Zhang[a], Tao Cheng[a], Bo Ren[a], Weizi Chen[a], Zibin Wang[a], Zhenzi Li[b,*], Wei Zhou[b,*]

[a] *Heilongjiang Provincial Key Laboratory of Environmental Nanotechnology, School of Chemistry and Materials Science, Heilongjiang University, Harbin 150080, P. R. China., Tel: +86-451-8660-8616, Fax: +86-451-8660-8240,*

Email: xingzipeng@hlju.edu.cn

[b] *Shandong Provincial Key Laboratory of Molecular Engineering, School of Chemistry and Chemical Engineering, Qilu University of Technology (Shandong Academy of Sciences), Jinan, Shandong, 250353, P. R. China*

Email: zzli@qlu.edu.cn; zwchem@hotmail.com

Experimental section

Materials

Bismuth nitrate pentahydrate ($Bi(NO_3)_3 \cdot 5H_2O$) was purchased from Tianjin Kemer Chemical Reagent Co., LTD. The 1, 3, 5-benzoic acid (H_3BTC), sodium molybdate dihydrate ($Na_2MoO_4 \bullet 2H_2O$), and thiouroid (CH_4N_2S) were purchased from Aladdin BioTechnologies Inc. Methanol (MeOH) and Silver nitrate ($AgNO_3$) were purchased from Shanghai Maclin Biochemical Technology Co., LTD.

Characterizations

The powder X-ray diffraction (XRD) patterns were acquired on a Bruker D8 Advance diffractometer by using Cu Kα radiation (λ = 1.5406 Å). Scanning electron micros-copy (SEM) images were obtained with a Philips XL-30-ESEM-FEG instrument operating at 20 kV. Transmission electron microscope (TEM) JEOL JEM-2010 at an accelerating voltage of 200 kV was also used to record the electron micrographs of the samples. X-ray photoelectron spectroscopy (XPS) was measured on a PHI-5700 ESCA instrument with Al-Kα X-ray source. UV-vis diffuse reflection spectra (DRS) were recorded on a UV-vis spectrophotometer (UV-2550, Shimadzu) with an integrating sphere attachment, and $BaSO_4$ was used as the reference material. Fourier transform infrared spectra (FT-IR) were detected with a PerkinElmer

spectrum one system. The N_2 adsorption-desorption isotherms at 77 K were collected on an AUTOSORB-1 (Quantachrome Instruments) nitrogen adsorption apparatus. Surface area was estimated by BET method and pore-size distribution was measured from the adsorption branch of the isotherm using the Barrett-Joyner-Halenda (BJH) method. The steady-state photoluminescence (PL) spectra were measured with a PE LS 55 spectrofluoro-photometer at excitation wavelength of 325 nm. Scanning Kelvin probe (SKP) measurements (SKP5050 system, Scotland) were performed at normal laboratory conditions. The electron spin resonance (ESR) spectra under visible light irradiation were tested with ESR spectrometer (Bruker model A300). The temperature of the sample was measured using the Testo 865 infrared thermograph.

Photocatalytic degradation

In order to test the photocatalytic ability under visible light irradiation (light source is 300 W Xenon lamp), we degrade Persistent Organic Dyes Rhodamine B at room temperature (20 ± 2 ^{o}C). In a typical experiment, 30 mg of photocatalyst and 15 mg of PMS was added to a Rhodamine B solution (30 mL, 10 mg L^{-1}), and then the suspension was placed in the dark for 30 min to ensure adsorption equilibrium. The suspension was irradiated with a 300 W Xenon lamp equipped with a filter ($\lambda \geq 420$ nm). The residual concentration of Rhodamine B was analyzed by a T6 UV-Vis

spectrophotometer.

Photocatalytic hydrogen evolution

The photocatalytic hydrogen evolution was tested in an online photocatalytic hydrogen evolution system (Au Light, Beijing, CEL-SPH2N) at room temperature. In a typical process, 50 mg of photocatalysts were suspended in 100 mL aqueous closed gas circulation reaction cell which include 80 mL deionized water and 20 mL of methanol used as the sacrificial reagent. Afterward, the suspension was purged with N_2 for several times to remove O_2 and CO_2. After that, the suspension solution was irradiated by a 300 W Xeon-lamp equipped with an AM 1.5 G filter (Oriel, USA), and use an on-line gas chromatography (SP7800, TCD, molecular sieve 5 Å, N_2 carrier, Beijing Keruida, Ltd) to analyze the hydrogen periodically with the interval of every 1h.

Photoelectrochemical measurements

Photoelectrochemical measurements of photocatalysts were detected in a three-electrode system with the CHI760E electrochemical workstation. The electrolyte selected KOH solution (1 M), the reference electrode selected Ag/AgCl and the opposite electrode selected Pt. Then, 0.1 g of photocatalysts were mixed with 3 mL of ethanol at stirring for 10 min, and sprayed on the FTO-glass of 1 × 2 cm^2 further

heating and drying. The photocurrent tests were extra monitored under AM 1.5G light exposure.

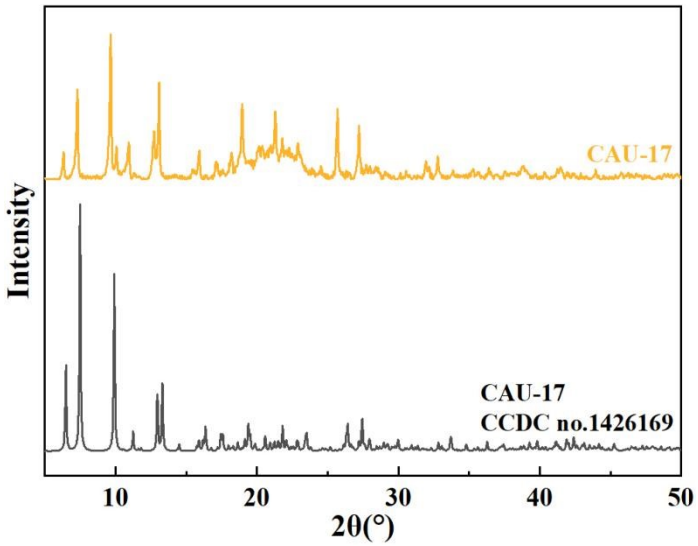

Figure S1. Standard XRD pattern of CAU-17.

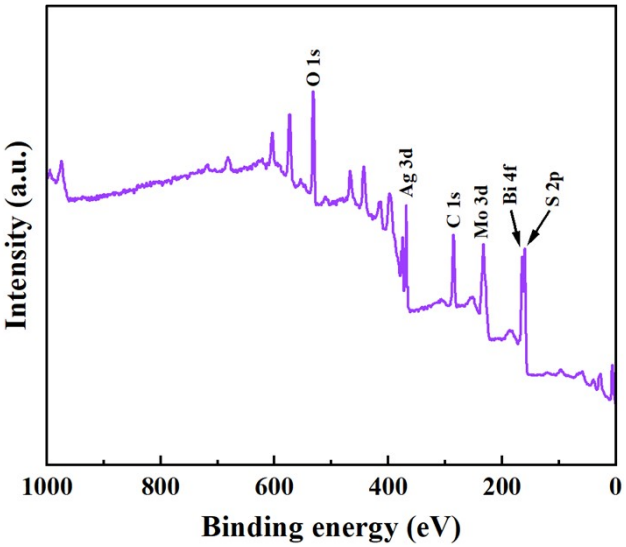

Figure S2. The XPS full scan of ACM.

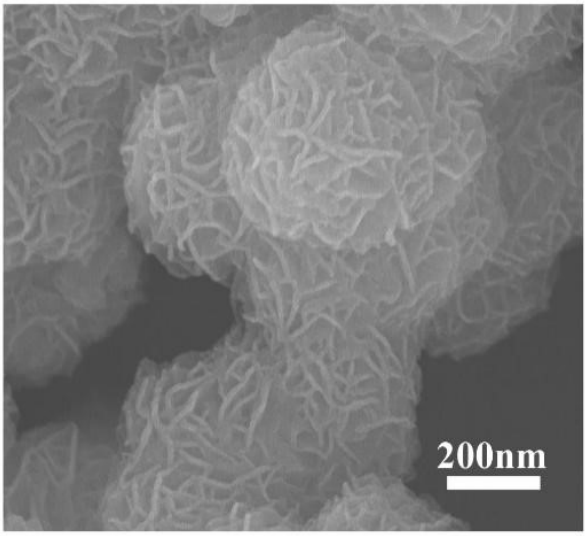

Figure S3. SEM image of MoS_2.

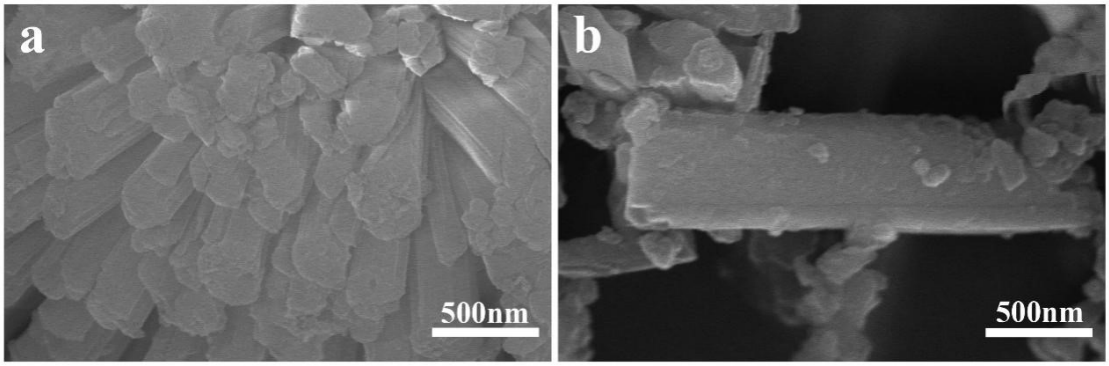

Figure S4. SEM image of CAU-17.

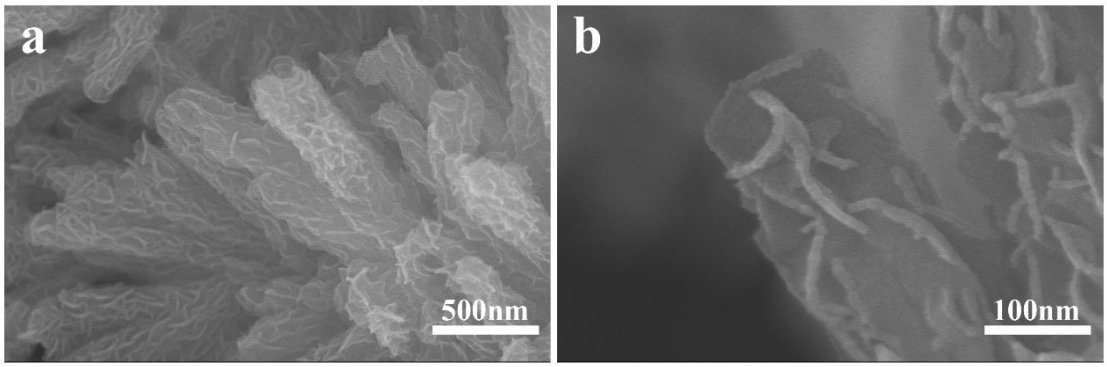

Figure S5. SEM image of ACM.

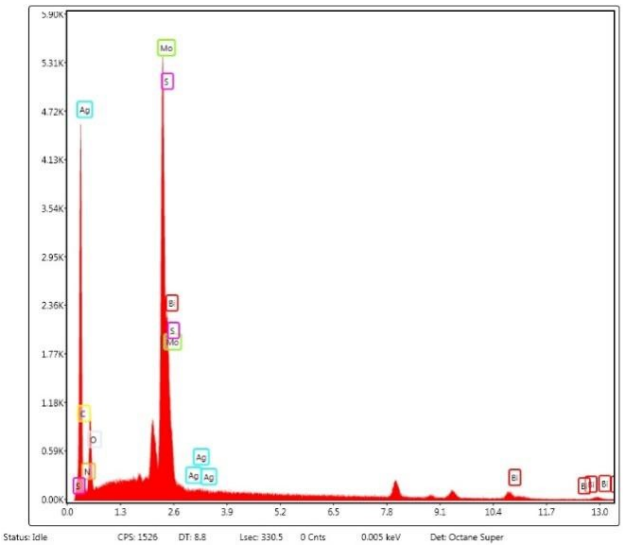

Figure S6. EDX spectrum of ACM.

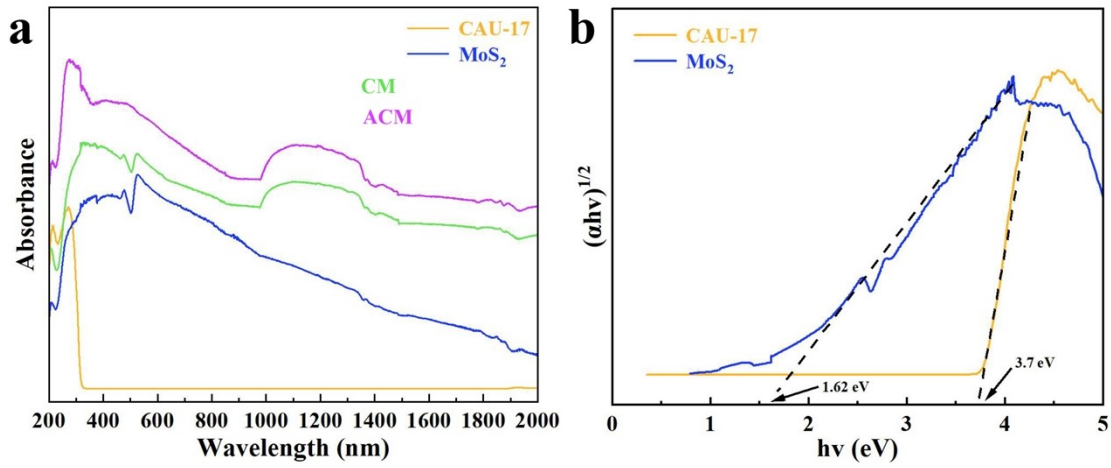

Figure. S7. (a) Ultraviolet spectra of CAU-17, MoS_2, CM and ACM, and band gap energies of CAU-17 and MoS_2 (b).

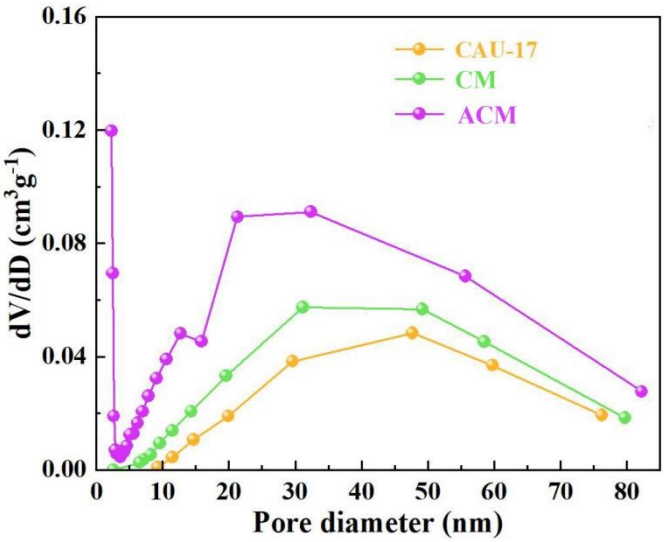

Figure S8. Pore size distributions for CAU-17, CM and ACM.

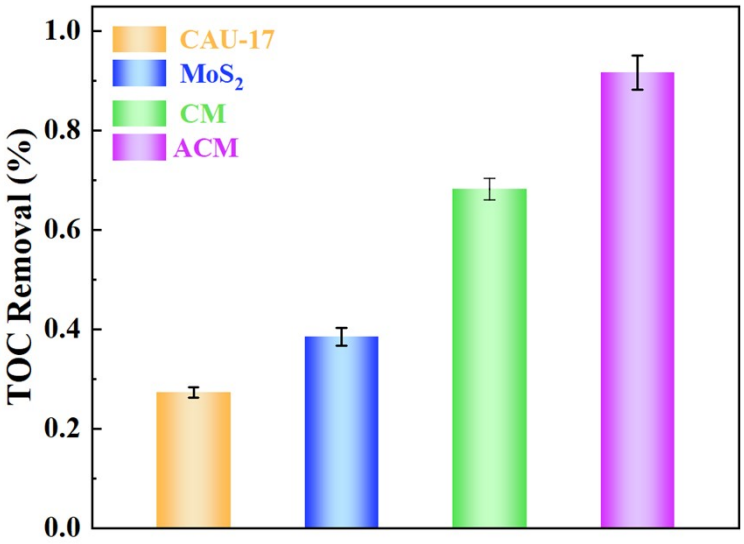

Figure. S9. TOC removal rates for tetracycline degradation in different samples.

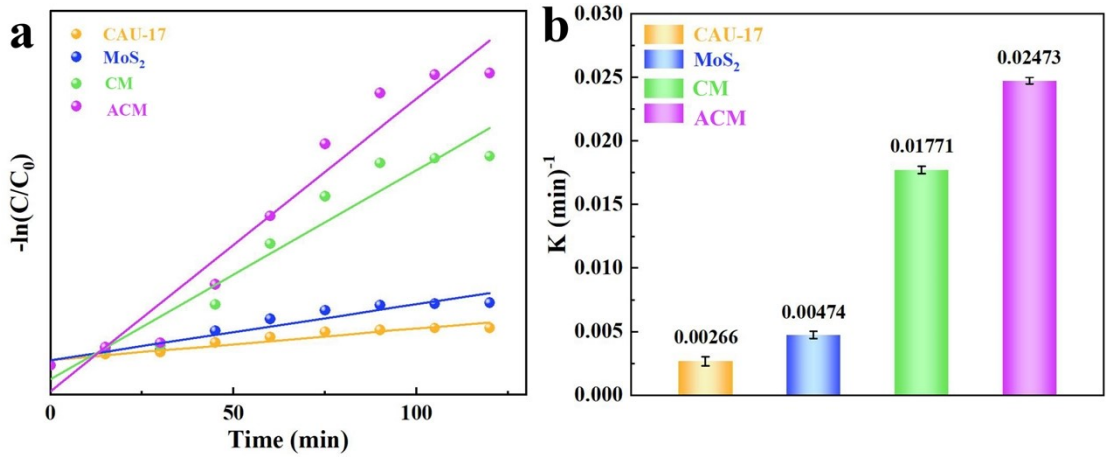

Figure S10. Quasi-first-order kinetic fitting curve (a) and apparent rate constant (b) for photocatalytic degradation of tetracycline by different photocatalysts.

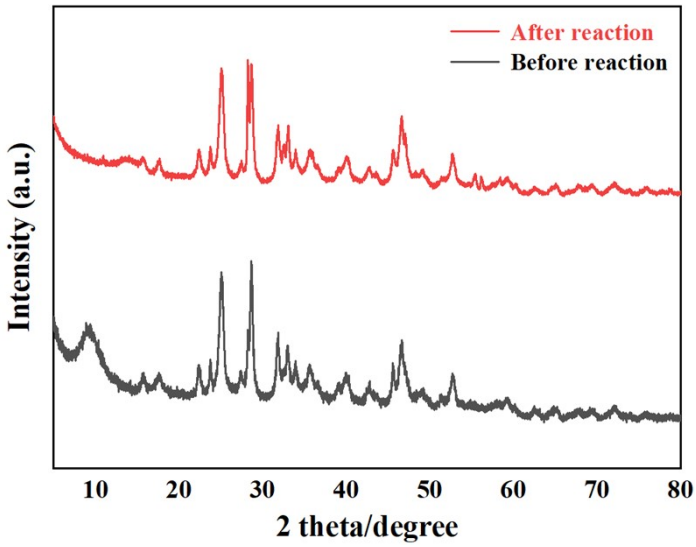

Figure S11. XRD patterns of ACM before and after the photocatalytic reaction.

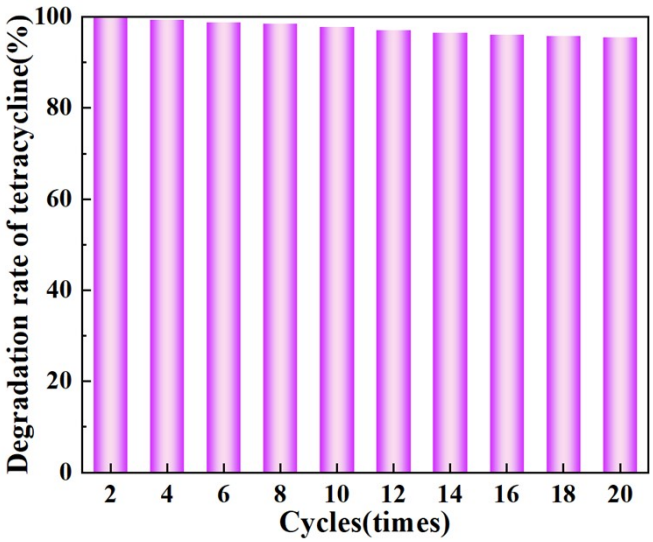

Figure. S12. Long-term stability test of photocatalytic degradation of tetracycline (20 cycles, 40 hours).

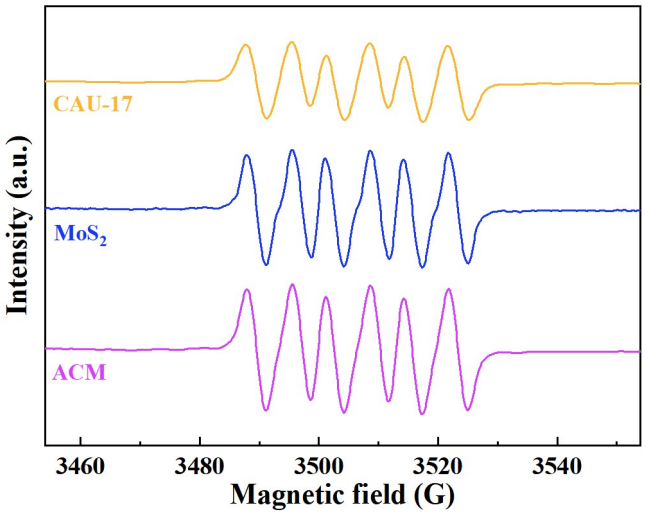

Figure S13. EPR signals of DMPO- $\cdot O_2^-$ in the presence of CAU-17, MoS_2, and ACM in light.

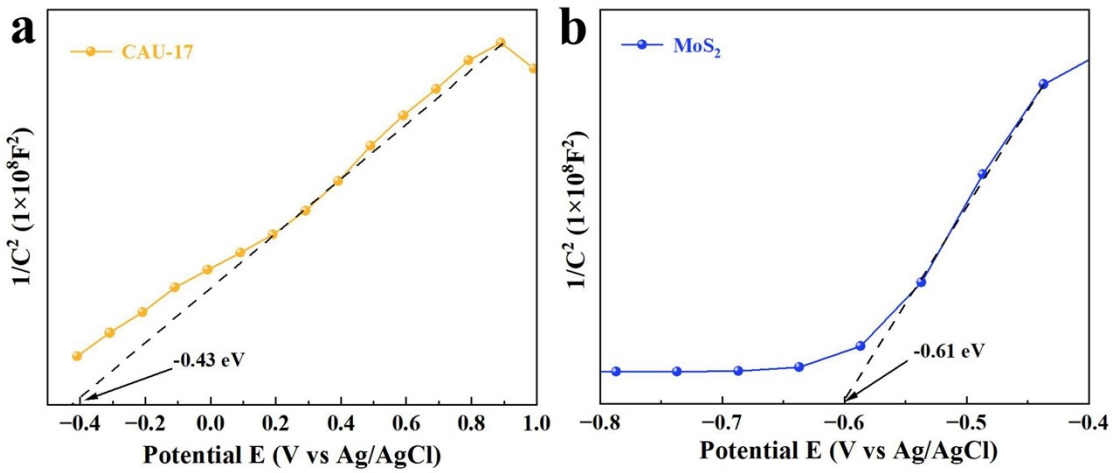

Figure S14. Mott-Schottky diagrams of CAU-17 (a) and MoS_2 (b).

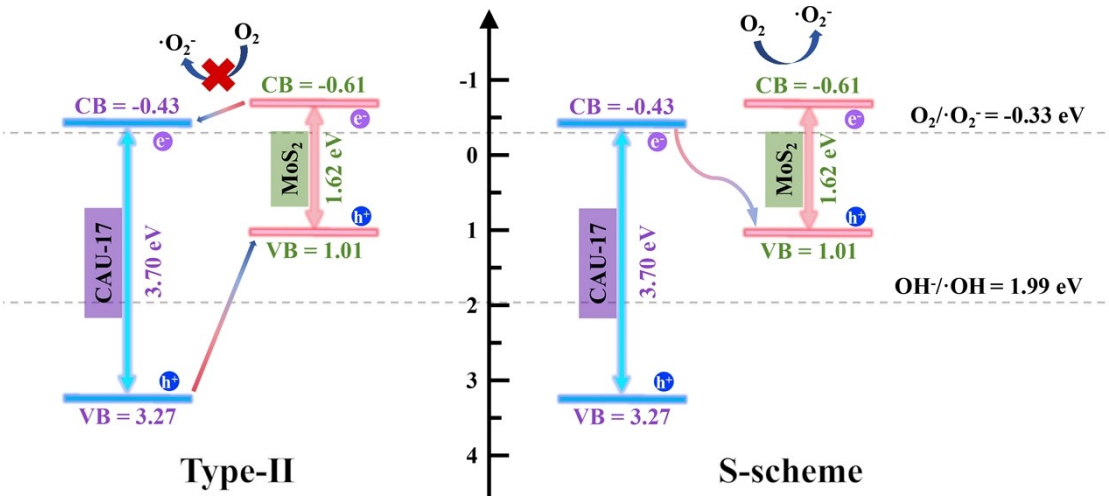

Figure. S15. Comparison of possible charge transfer mechanisms (type II and type S) of ACM under visible light irradiation.

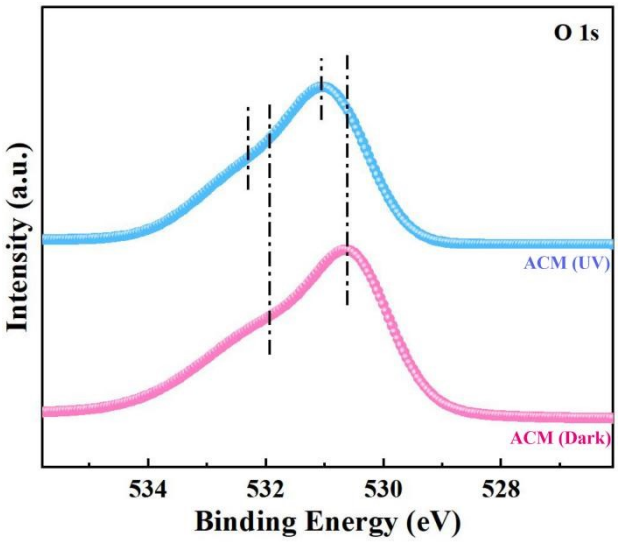

Figure S16. In situ XPS spectra of O 1s by ACM under dark ultraviolet irradiation.

Table S1. Results of the exponential decay-fitted parameters for the fluorescence lifetimes of as-prepared samples.

Samples	τ_1(ns)	A_1	τ_2(ns)	A_2	τ(ns)
CAU-17	0.80	0.59	4.15	0.27	3.18
MoS_2	0.51	0.61	2.59	0.18	1.76
CM	0.80	0.64	4.40	0.24	3.22
ACM	1.03	0.66	5.04	0.26	3.67

Table S2. The ratio between the specific surface of the catalyst and the rate of hydrogen production.

Photocatalyst	BET surface surface (m^2 g^{-1})	H_2 evolution rate	Normalized the relationship
CAU-17	83.31 m^2 g^{-1}	26.3 μmol $h^{-1}g^{-1}$	0.316
CM	93.91 m^2 g^{-1}	274.4 μmol h^{-1} g^{-1}	2.921
ACM	108.26 m^2 g^{-1}	326.5 μmol $h^{-1}g^{-1}$	3.016

Table S3. The photocatalytic H_2 evolution rates of different photocatalysts.

Photocatalyst	Light source	H_2 evolution rate	Refs.
Ag-In-S QDs/ $Co(bpy)_3^{2+}$	300 W Xe lamp (λ>420 nm)	3.13 μmol $h^{-1}g^{-1}$	[1]
Bi-OVs-$Bi_4O_5Br_2$	300 W Xe lamp (λ>420 nm)	67.9 μmol $h^{-1}g^{-1}$	[2]
Bi_2S_3/g-C_3N_4	300 W Xe lamp (λ>420 nm)	236.1 μmol $h^{-1}g^{-1}$	[3]
$Co_{1.8}$-BFO	300 W Xe lamp (λ>420 nm)	321.9 μmol $h^{-1}g^{-1}$	[4]
C-MoS_2/g-C_3N_4	300 W Xe lamp (λ>420 nm)	157.14 μmol $h^{-1}g^{-1}$	[5]
MoS_2/g-C_3N_4	300 W Xe lamp (λ>420 nm)	280 μmol $h^{-1}g^{-1}$	[6]
Pt–P@CN	300 W Xe lamp (λ>420 nm)	138 μmol h^{-1} g^{-1}	[7]
ACM	**300 W Xe lamp (λ>420 nm)**	**326.5 μmol $h^{-1}g^{-1}$**	**This work**

Table S4. The band gap energies (E_g), conduction band (CB) and valence band (VB) potentials (NHE) for CAU-17 and MoS_2.

Samples	E_g (eV)	CB (V)	VB (V)
CAU-17	3.70	-0.43	3.27
MoS_2	1.62	-0.61	1.01

[1] L. Shi, X. Ren, Z. Zhang, Q. Wang, Y. Li, J. Ye, Non-stoichiometric Ag-In-S quantum dots for efficient photocatalytic CO_2 reduction: Ag/In molar ratio dependent activity and selectivity, J. Catal., 401 (2021) 271-278.

[2] L. Zhao, W. Fang, X. Meng, L. Wang, H. Bai, C. Li, In-situ synthesis of metal Bi to improve the stability of oxygen vacancies and enhance the photocatalytic activity of $Bi_4O_5Br_2$ in H_2 evolution, J. Alloys Compd., 910 (2022) 164883.

[3] Y. Li, F. Rao, J. Zhong, J. Li, In-situ fabrication of Bi_2S_3/g-C_3N_4 heterojunctions with boosted H_2 production rate under visible light irradiation, Fuel, 341 (2023) 127629.

[4] Y. Wang, M. Yang, K. Cui, L. Zhang, X. Wang, S. Ge, J. Yu, Z. Cheng, Band Engineering of $BiFeO_3$ Nanosheet for Boosting Hydrogen Evolution by Synergetic Piezo-photocatalysis, ACS Sustainable Chem. Eng., 12 (2024) 2300-2312.

[5] X. Wei, X. Zhang, S. Ali, J. Wang, Y. Zhou, H. Chen, G. Zhang, J. Qi, D. He, Carbon intercalated MoS_2 cocatalyst on g-C_3N_4 photo-absorber for enhanced photocatalytic H_2 evolution under the simulated solar light, Int. J. Hydrogen Energy, 48 (2023) 13827-13842.

[6] Y. Liu, X. Xu, H. Li, Z. Si, X. Wu, R. Ran, D. Weng, A Facile One Step Synthesis of MoS_2/g-C_3N_4 Photocatalyst with Enhanced Visible Light Photocatalytic Hydrogen Production, Catal. Lett., 152 (2022) 972-979.

[7] X. Zhou, Y. Liu, Z. Jin, M. Huang, F. Zhou, J. Song, J. Qu, Y.-J. Zeng, P.-C. Qian, W.-Y. Wong, Solar-Driven Hydrogen Generation Catalyzed by g-C3N4 with Poly(platinaynes) as Efficient Electron Donor at Low Platinum Content, Adv. Sci. Lett., 8 (2021) 2002465.